BIOCHEMISTRY
including biophysical chemistry & molecular biology

Article

pubs.acs.org/biochemistry

Inhibition of *Escherichia coli* Respiratory Complex I by Zn^{2+}

Marius Schulte,[†] Dinah Mattay,[†,§] Sebastien Kriegel,[‡,∥] Petra Hellwig,[‡] and Thorsten Friedrich*[,†]

[†]Institut für Biochemie, Albert-Ludwigs-Universität, 79104 Freiburg, Germany

[‡]Laboratoire de bioelectrochimie et spectroscopie, UMR 7140, Chimie de la Matière complexe, CNRS, Université de Strasbourg, 67070 Strasbourg, France

ABSTRACT: The energy-converting NADH:ubiquinone oxidoreductase, respiratory complex I, couples NADH oxidation and quinone reduction with the translocation of protons across the membrane. Complex I exhibits a unique L shape with a peripheral arm extending in the aqueous phase and a membrane arm embedded in the lipid bilayer. Both arms have a length of ∼180 Å. The electron transfer reaction is catalyzed by a series of cofactors in the peripheral arm, while the membrane arm catalyzes proton translocation. We used the inhibition of complex I by zinc to shed light on the coupling of the two processes, which is not yet understood. Enzyme kinetics revealed the presence of two high-affinity binding sites for Zn^{2+} that are attributed to the proton translocation pathways in the membrane arm. Electrochemically induced Fourier transform infrared difference spectroscopy demonstrated that zinc binding involves at least two protonated acidic residues. Electron paramagnetic resonance spectroscopy showed that one of the cofactors is only partially reduced by NADH in the presence of Zn^{2+}. We conclude that blocking the proton channels in the membrane arm leads to a partial block of the electron transfer in the peripheral arm, indicating the long-range coupling between both processes.

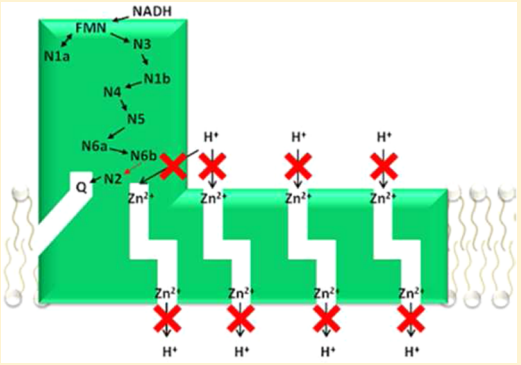

The NADH:ubiquinone oxidoreductase, respiratory complex I, is the first and largest enzyme complex of the respiratory chains of many eukaryotes and most bacteria. It couples the transfer of two electrons from NADH to ubiquinone with the translocation of four protons across the membrane.[1−5] Dysfunctions of the human complex I are related to the onset of neurodegenerative diseases such as Parkinson's or Alzheimer's disease and of aging.[6,7] The bacterial complex comprises 13−16 subunits called NuoA−N or Nqo1−16. They add up to a molecular mass of ∼550 kDa.[8,9] Complex I has an unusual L-shaped structure consisting of a peripheral arm and a membrane arm. Recently, the structure of the *Thermus thermophilus* complex was determined at 3.3 Å resolution.[10] The peripheral arm harbors one flavin mononucleotide (FMN) and, depending on the species, 8−10 iron−sulfur (Fe/S) clusters called N1a to N6b (Figure 1). Electrons from NADH are transferred to the flavin and from there via a chain of seven Fe/S clusters to the substrate quinone. The quinone-binding site is located at the interface of the two arms. The membrane arm contains four putative proton translocation pathways built up by two half-channels each.[10] It is suggested that the redox reaction in the peripheral arm induces conformational changes that are transmitted to the membrane arm leading to the opening and closing of the individual half-channels.[10]

Zinc is an essential micronutrient acting as a cofactor in many proteins. However, high concentrations of Zn^{2+} are toxic because they induce the death of neurons.[11] In addition, Zn^{2+} is known to inhibit the production of cell energy by affecting the

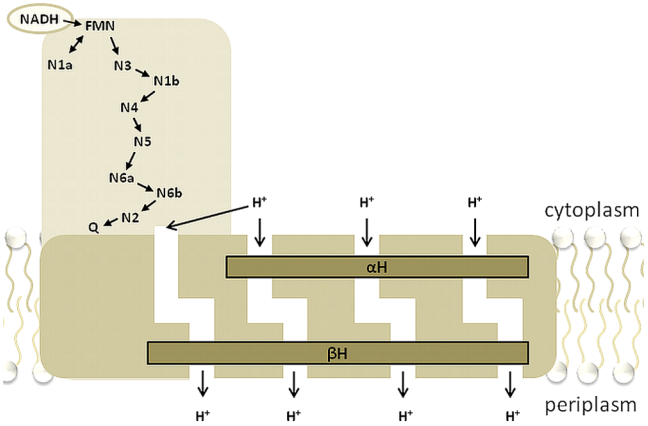

Figure 1. Scheme of respiratory complex I as derived from structural data.[10] The approximate positions of the FMN and Fe/S clusters N1a, N1b, N2−N5, N6a, and N6b are provided as well as the binding sites for NADH and the quinone (Q). The positions of the four proton translocation pathways consisting of two half-channels each are indicated. The positions of the membrane arm stabilizing elements on both sides of the membranes, αH and βH, are given. Their role in proton translocation is under discussion.[10]

glyceraldehyde-3-phosphate dehydrogenase in glycolysis,[12] the α-ketoglutarate dehydrogenase complex in the TCA cycle,[13]

Received: July 28, 2014
Revised: September 18, 2014
Published: September 19, 2014

   dx.doi.org/10.1021/bi5009276 | *Biochemistry* 2014, 53, 6332−6339

and respiratory complexes I,[14] III,[15] and IV.[16−18] It was shown that zinc interferes with the reduction and protonation of quinone and/or proton translocation in complexes I and III[14,15] and inhibits proton translocation in complex IV.[16−18] Here, we use the inhibition of complex I by Zn^{2+} to elucidate the coupling of the redox reaction in the peripheral arm with proton translocation in the membrane arm.

MATERIALS AND METHODS

Protein Preparation and Determination of Enzymatic Activities. Complex I was isolated from an overproducing strain as described previously.[19] The NADH:decyl-ubiquinone oxidoreductase activity of the preparation was measured as a decrease in the NADH concentration at 340 nm using an ε of 6.2 mM^{-1} cm^{-1}. The enzyme (10 mg/mL) was mixed with *Escherichia coli* polar lipids (10 mg/mL, Avanti) in a 1:1 (w/w) ratio and incubated for 20 min on ice. One microliter of the protein/lipid mixture and 60 μM decyl-ubiquinone were added to the assay buffer [50 mM MES-NaOH and 50 mM NaCl (pH 6.0)]. The mixture was incubated for 1 min at 30 °C, and the reaction was started by an addition of NADH at various concentrations. The activity of this preparation is ∼3.3 units/mg, while higher activities are reported for other preparations of *E. coli* complex I. However, we have demonstrated that this activity is more than 95% inhibited by piericidin A, a specific complex I inhibitor, and that the rate of quinone reduction is virtually identical to that of NADH oxidation. Thus, the physiological activity is measured with the overproduced enzyme.[35] The NADH/hexaammineruthenium(III) oxidoreductase activity was determined in the same way but with 0.5 μg of complex I and using 1 mM hexaammineruthenium(III) chloride as an electron acceptor.

EPR Spectroscopy. EPR measurements were taken with an EMX 6/1 ESR spectrometer (Bruker) operating at X-band. The sample temperature was controlled with an ESR-9 helium flow cryostat (Oxford Instruments). The magnetic field was calibrated using a strong pitch standard. Spectra were recorded at 13 K at a microwave power of 5 mW. Other experimental conditions are provided in the figure legends. Complex I (10 μM) was incubated with either 250 μM $ZnCl_2$ or the same volume of buffer for 3 min, and both samples were reduced by an addition of 500 μM NADH.

FT-IR Spectroscopy. The samples for FT-IR spectroscopy were in 50 mM MES, 50 mM NaCl, and 0.01% DDM (pH 6.3). One microliter of a 0.1 M $ZnSO_4 \cdot H_2O$ solution (Sigma-Aldrich) in the same buffer was added to 7 μL of complex I (80 mg/mL). The samples were incubated for 3 h at 4 °C. The ultrathin layer spectroelectrochemical cell was used as described previously.[20] To avoid irreversible protein adhesion, the gold grid working electrode was modified by incubation with a 2 mM cysteamine and mercaptopropionic acid solution for 1 h and then washed with deionized water. To accelerate the redox reactions, a mixture of 19 mediators[20] was added at substoichiometric concentrations of 40 μM each to the protein solution; 7−8 μL of the solution was used to fill the electrochemical cell. The cell path length was <10 μm, as determined at the beginning of each experiment. All experiments were performed at 278 K. FT-IR spectra were recorded as a function of the applied potential using a setup combining an IR beam from the interferometer (Vertex 70, Bruker) for the 4000−1000 cm^{-1} range. First, the protein was equilibrated at an initial electrode potential, and a single-beam spectrum was recorded. Then the final potential was applied, and a single-beam spectrum was again recorded after equilibration. Equilibration generally took 8 min for the full potential step from −500 to 200 mV (vs the SHE). Difference spectra as presented here were calculated from two single-beam spectra, with the initial spectrum taken as a reference. Typically, 2 × 256 interferograms at 4 cm^{-1} resolution were co-added for each single-beam spectrum and Fourier transformed using triangular apodization and a zero filling factor of 2. Sixty difference spectra were averaged.

RESULTS AND DISCUSSION

Inhibition of *E. coli* Complex I by Cations. The effect of a variety of cations on complex I activity was inspected by incubating the complex with various salts at 500 μM for 1 min before its NADH:decyl-ubiquinone oxidoreductase activity was assayed. The monovalent cations Li^+, Na^+, K^+, and Cs^+ had a very slight effect on activity, which was also true for the divalent cations Mg^{2+}, Ca^{2+}, Mn^{2+}, Co^{2+}, and Ni^{2+} (Figure 2). Gd^{3+}

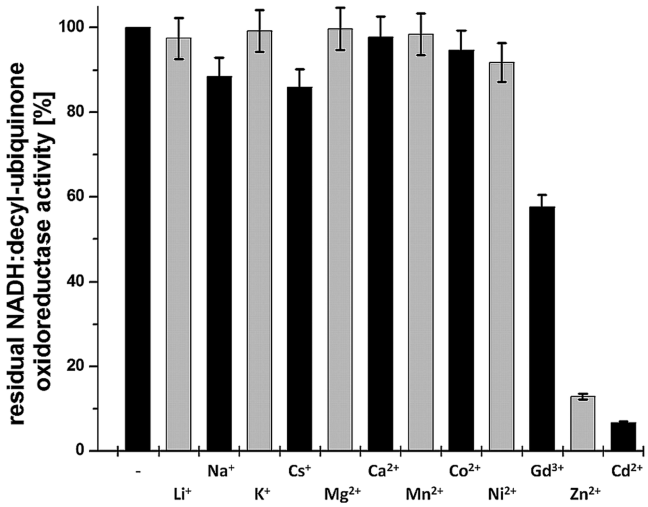

Figure 2. Effect of various cations on the NADH:decyl-ubiquinone oxidoreductase activity of complex I. The residual activity after incubation with the corresponding cation at 500 μM for 1 min on ice is shown. The activity of the untreated sample is 3.3 units/mg.

inhibited complex I activity by one-third. A significant inhibition of ∼90% was achieved by an addition of Cd^{2+} and Zn^{2+}. The inhibition did not depend on the chemical nature of the counterion as the chlorides showed the same inhibitory competence as the sulfates. It is known that low concentrations of these cations inhibit proton-translocation pathways in several proteins. Crystallographic studies with the *Rhodobacter sphaeroides* cytochrome *c* oxidase showed that Cd^{2+} and Zn^{2+} bind to charged amino acids at both ends of the pathway.[18]

Inhibition of the NADH:Decyl-ubiquinone Oxidoreductase Activity by Zn^{2+}. The addition of Zn^{2+} led to a progressive decrease in the NADH:decyl-ubiquinone oxidoreductase activity of complex I over time (Figure 3), which can be explained either by a low binding rate constant or by a binding site that is only accessible in distinct enzymatic state(s). The IC_{50} values of Zn^{2+} inhibition after incubation of the complex with Zn^{2+} for 20 min and for 20 s were similar (55 ± 5 and 50 ± 5 μM, respectively), pointing to the presence of binding site(s) that are accessible only in a distinct enzymatic state.

dx.doi.org/10.1021/bi5009276 | *Biochemistry* 2014, 53, 6332−6339

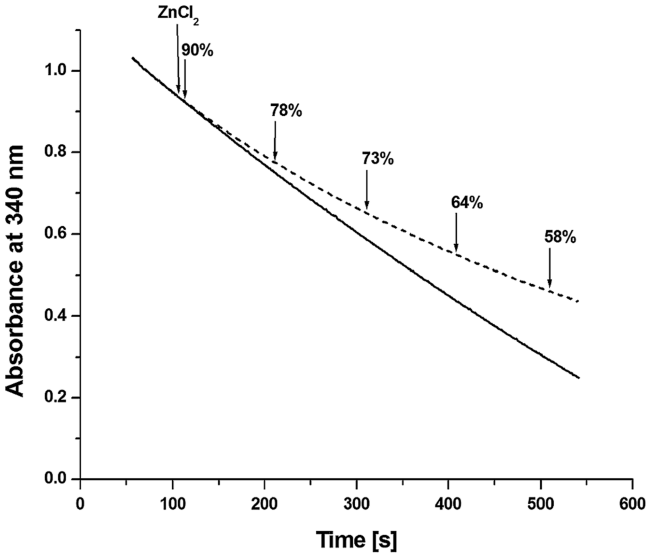

Figure 3. Progressive inhibition of the NADH:decyl-ubiquinone oxidoreductase activity of complex I by Zn^{2+}. The activity of an untreated sample (—) and of an aliquot treated with 20 μM $ZnCl_2$ (---) is shown. The addition of $ZnCl_2$ is marked by an arrow, and the residual activity of the Zn^{2+}-treated sample at distinct times (also indicated by arrows) is given.

The IC_{50} value of Zn^{2+} on the NADH:decyl-ubiquinone oxidoreductase activity strongly increased at a lower pH, indicating that either Zn^{2+} competes with the binding of protons or the complex adopts a different conformation at this pH, hindering Zn^{2+} binding (Figure 4). Because of the

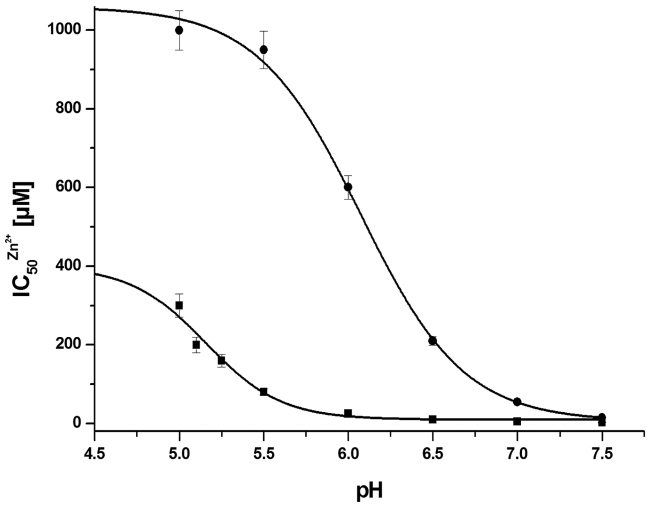

Figure 4. Dependence of the IC_{50} of Zn^{2+} inhibition of NADH:decyl-ubiquinone oxidoreductase activity (■) and NADH/HAR oxidoreductase activity (●) on pH. The data points were fit with a Boltzmann function assuming a plateau of 400 μM for the NADH:decyl-ubiquinone oxidoreductase activity.

instability of the preparation at acidic pH values, no data below pH 5.0 were obtained. Assuming a sigmoidal shape with a plateau at ~400 μM Zn^{2+}, an inflection point of at least pH 5.2 is derived. If a higher maximal IC_{50} were obtained, the inflection point would be a bit lower. Thus, the value of 5.2 is an upper limit, and the actual inflection point might actually be at a more acidic pH. This is compatible with a binding of Zn^{2+} to residue(s) containing carboxylates in hydrophobic surroundings (see below).

To judge whether Zn^{2+} competes with the binding of the substrates, the K_m for NADH and quinone at various Zn^{2+} concentrations was determined (Figure 5). As the K_m for decyl-

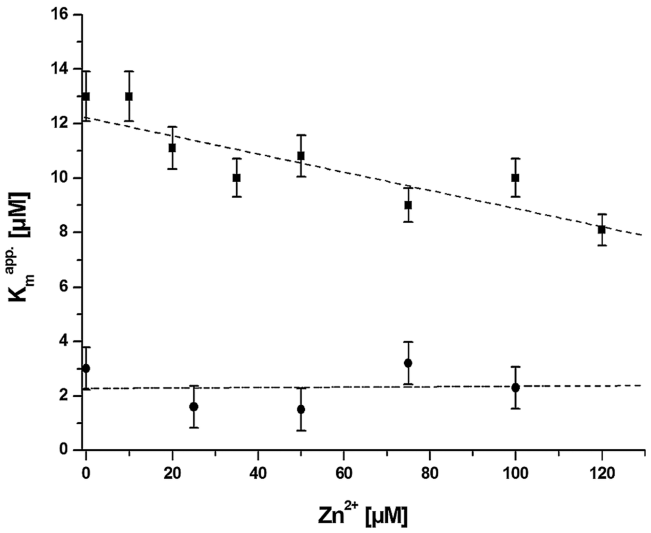

Figure 5. Effect of increasing Zn^{2+} concentrations on the K_m of complex I with respect to NADH (■) and decyl-ubiquinone (●) measured as NADH:decyl-ubiquinone oxidoreductase activity. The activity of the untreated sample is 3.3 units/mg. The dotted lines through the data points are included only as a guide.

ubiquinone remained unchanged, the binding, reduction, and protonation of decyl-ubiquinone are not affected by Zn^{2+}. However, the K_m toward NADH slightly decreased at increasing Zn^{2+} concentrations (Figure 5).

Inhibition of the NADH/Hexaammineruthenium Oxidoreductase Activity. The influence of Zn^{2+} on NADH binding was assayed using the NADH/hexaammineruthenium-(III) (HAR) oxidoreductase activity. This artificial activity involves only the FMN cofactor and the bound nucleotide.[21] Thus, the reaction includes neither transfer of electrons to the quinone nor proton translocation. The NADH/HAR oxidoreductase activity was determined at various Zn^{2+} concentrations (Figure 6). The Lineweaver–Burk plot shows an intercept at the abscissa, indicating noncompetitive inhibition. Plotting the ordinate intercepts against the inhibitor concentration (Figure 6) reveals a K_i^{HAR} of 720 ± 10 μM. The high K_i and the noncompetitive type of inhibition with respect to NADH clearly show that binding of Zn^{2+} to the NADH-binding site is not causative for the inhibition of the complex but indicate the presence of an additional, low-affinity binding site of Zn^{2+}. This assumption is supported by the pH dependency of the IC_{50} values of the NADH/HAR oxidoreductase reaction (Figure 4). The sigmoidal shape with its inflection point at pH 6.2 denotes that Zn^{2+} probably binds to histidine residue(s). However, as mentioned above, the possibility that the change in pH results in a different conformation of the protein resulting indirectly in a changed accessibility of the binding site cannot be excluded.

Determination of the High-Affinity Binding Site. To identify the high-affinity binding site(s), the enzymatic activity was measured at various NADH and Zn^{2+} concentrations. The data were evaluated in a Lineweaver–Burk diagram (Figure 7) showing that the regression lines intersect in the second quadrant. This is indicative of a mixed inhibition comprising

dx.doi.org/10.1021/bi5009276 | Biochemistry 2014, 53, 6332–6339

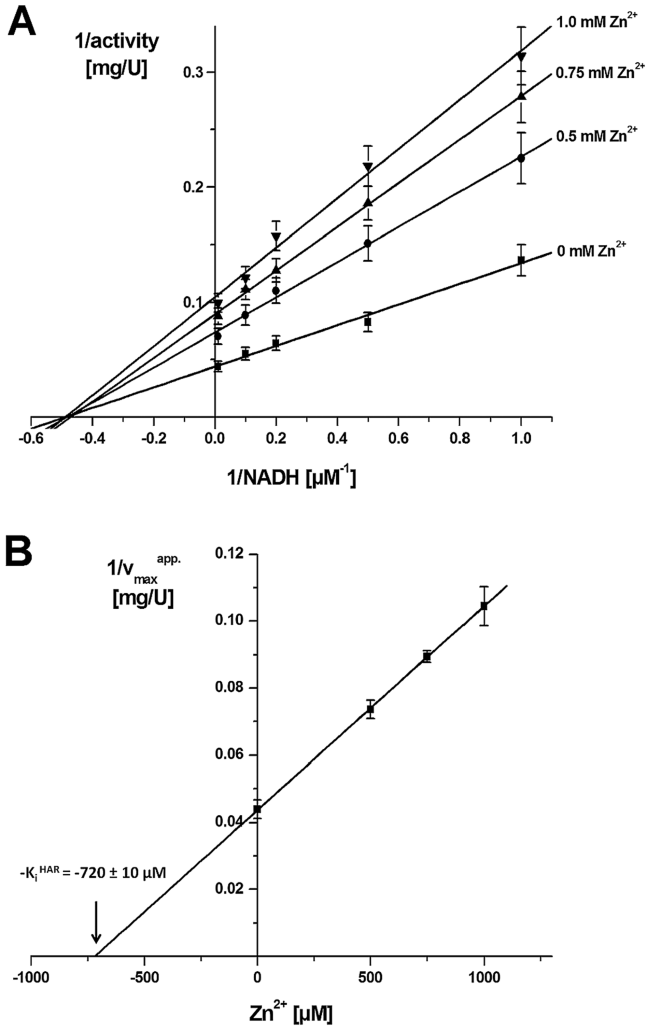

Figure 6. (A) Lineweaver–Burk plot of the NADH/HAR oxidoreductase activity at various Zn^{2+} concentrations and (B) double-reciprocal plot of the corresponding ordinate intercepts. The Lineweaver–Burk plot shows the linearization of the Michaelis–Menten curves at 0 μM (black), 500 μM (red), 750 μM (green), and 1 mM (blue) Zn^{2+}. The regression curve of the double-reciprocal plot intercepts the abscissa at a $-K_i^{HAR}$ of -720 ± 10 μM.

two different inhibition constants, K_{ic} and K_{iu}, according to the kinetic model depicted in Scheme 1. In this model, the enzyme and the enzyme/substrate complex show a distinct affinity for the inhibitor characterized by inhibition constants K_{ic} and K_{iu}.

K_{ic} and K_{iu} were determined using a double-reciprocal plot of the ordinate intercepts and the slopes of the Lineweaver–Burk linearization, respectively, versus Zn^{2+} concentration. The abscissa intercepts reveal a K_{ic} of 50 ± 3 μM and a K_{iu} of 86 ± 2 μM (Figure 7A). As a control, the K_{ic} was also calculated from a Dixon plot (Figure 7B), yielding a K_{ic} of 45 ± 5 μM. This indicates the presence of two high-affinity Zn^{2+}-binding sites that are accessible in only a distinct conformation of the complex. Alternatively, the mixed inhibition is indicative of two different states of the same site. However, it is not possible to distinguish between these possibilities by enzyme kinetics.

Interactions of Zn^{2+} with specific residues were monitored by recording FT-IR redox difference spectra of the complex in the absence and presence of Zn^{2+} (Figure 8). A fully reversible redox reaction was observed for both samples. The double-difference spectra obtained by subtracting the spectra in the presence of Zn^{2+} from those without Zn^{2+} show clear differences (Figure 8).

Signals in the spectral range above 1710 cm^{-1} are characteristic for the ν(C=O) vibrational mode of protonated aspartate or glutamate side chains.[22,23] The high frequency of the signals at 1781 and 1763 cm^{-1} corresponds to a protonated acidic residue in a highly hydrophobic environment, as reported for other enzymes.[24,25] Because of the presence of two distinct signals above 1710 cm^{-1}, it is suggested that at least two acidic residues are protonated upon oxidation of the complex in the presence of Zn^{2+} that are not protonated or addressed by the redox reaction in the absence of Zn^{2+}.

Contributions of the $\nu(COO^-)^{as}$ of the deprotonated acidic residues are typically in the range from 1590 to 1520 cm^{-1}, whereas $\nu(COO^-)^{s}$ can be expected to be between 1490 and 1320 cm^{-1}.[22,23] When ions bind, the positions shift by several wavenumbers, the exact shifts depend on the binding mode. This was previously described for the interaction of COO^- groups with Na^+ ions.[26,27] Clearly, signals between 1590 and 1520 cm^{-1} are perturbed upon binding of Zn^{2+}, revealing that $\nu(COO^-\cdots Zn^{2+})$ vibrations are seen in the spectra. However, in addition to the contributions of the COO^- groups, contributions of the coupled ν(CN/NH) vibration from the protein backbone may be involved here. They can be differentiated upon H/D exchange, because the uncoupled CN and ND vibrations are expected at significantly lower frequencies.[28] Approximately 40% of the signals obtained in the presence of Zn^{2+} remain unperturbed in D_2O, confirming the assignment to COO^- vibrations.

Shifts in the spectra of the Zn^{2+}-treated sample at 1677, 1659, 1648, and 1635 cm^{-1} in the amide I range include the ν(C=O) vibration of the polypeptide backbone.[29,30] They may be partially assigned to a small perturbation of conformational changes. However, it is noted that individual amino acids also contribute here.[22,23]

Inhibition of the Electron Transfer. EPR spectra of the complex in the presence and absence of Zn^{2+} were recorded to detect a possible effect on the intramolecular electron transfer between the Fe/S clusters (Figure 9). In the presence of Zn^{2+}, the most distal cluster, N2, is reduced by NADH to only 65%, comparing the signal's amplitude with that of the untreated sample as highlighted in the difference spectrum (Figure 9C). Chemical reduction by dithionite leads to identical spectra for both samples (Figure 9), indicating that the partial reduction of N2 in the presence of Zn^{2+} is not due to a partial loss of the cluster. The NADH:decyl-ubiquinone oxidoreductase activity is inhibited by more than 80% at that Zn^{2+} concentration, demonstrating that the hampered reduction of N2 is not the reason for the inhibitory effect of Zn^{2+}. Instead, we suggest that blocking the proton translocation pathway(s) by Zn^{2+} as reported previously[14] leads to an impeded structural rearrangement around N2 that is needed for its physiological reduction by NADH. This would provide a functional role for the conformational changes in the environment of N2 that have been detected in structural studies.[31]

CONCLUSIONS

Zn^{2+} inhibits various enzyme complexes of the respiratory chains.[14−18] Here, we demonstrate that Zn^{2+} also inhibits the bacterial complex I from *E. coli* with high affinity. The detailed kinetic and spectroscopic analysis of Zn^{2+} binding shows that Zn^{2+} has several binding sites at *E. coli* complex I. Zn^{2+} binds to a low-affinity site characterized by a K_i^{HAR} of 720 μM. However,

dx.doi.org/10.1021/bi5009276 | *Biochemistry* 2014, 53, 6332−6339

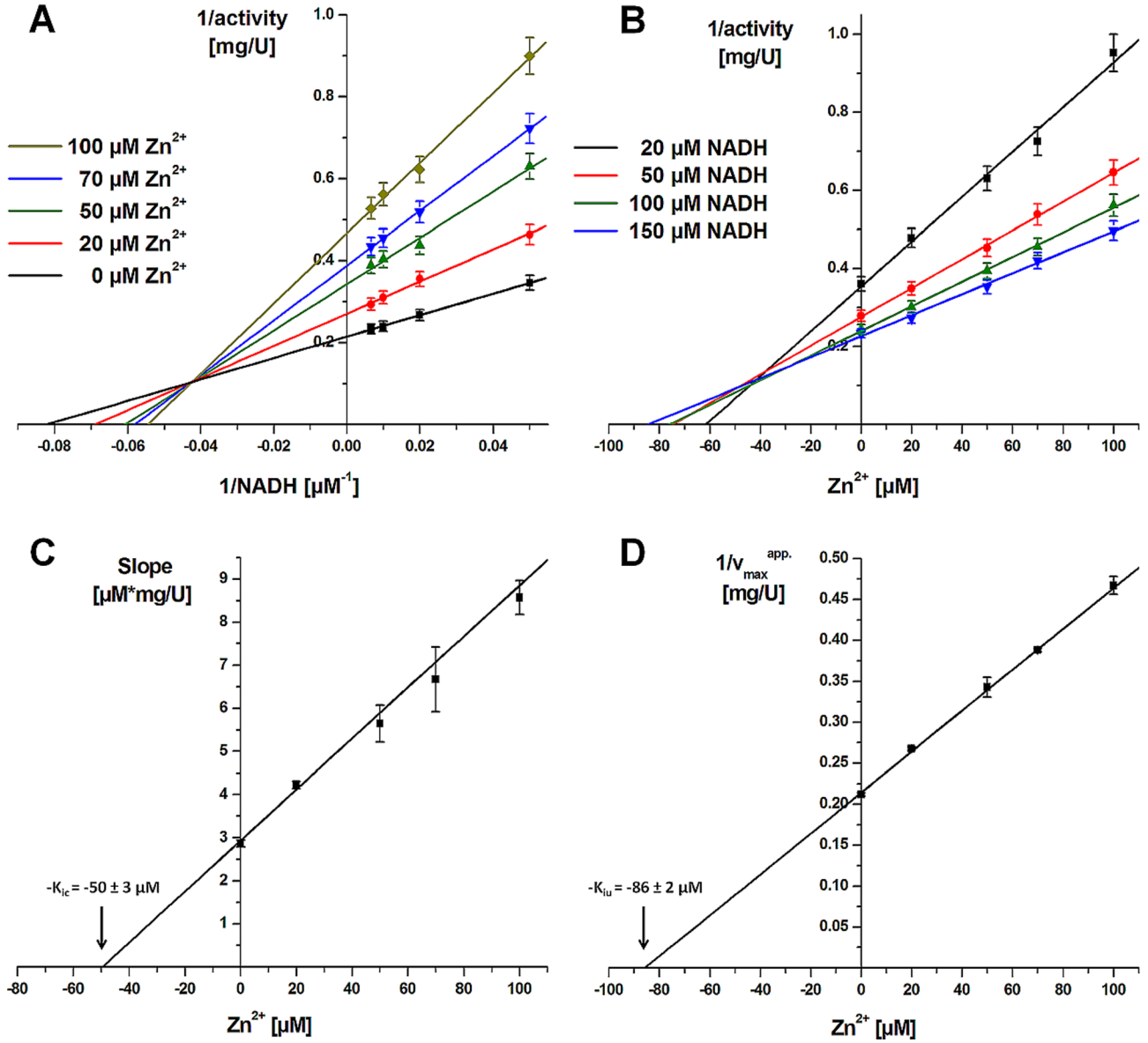

Figure 7. (A) Lineweaver–Burk plot of the NADH:decyl-ubiquinone oxidoreductase activity at various Zn^{2+} and NADH concentrations. The Lineweaver–Burk linearization of the activity in the presence of Zn^{2+} shows an intersection of the partial regression lines in the second quadrant indicating a mixed inhibition. (B) The corresponding Dixon plot at various NADH concentrations gives a K_{ic} value of 45 ± 5 μM. (C and D) The plot of the slopes of the linearized Lineweaver–Burk and the ordinate intercepts ($1/v_{max}$), respectively, show a K_{iu} of 86 ± 2 μM and a K_{ic} of 50 ± 3 μM.

Scheme 1. Kinetic Model of Binding of Zn^{2+} to Complex I

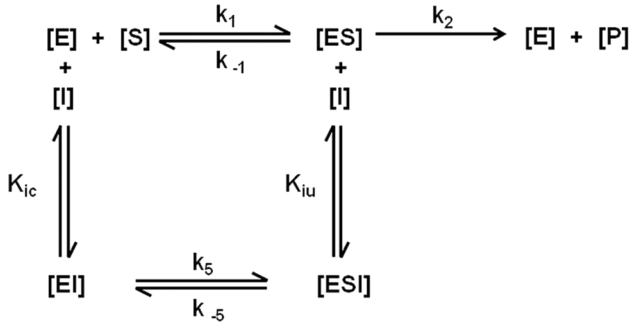

inhibition of complex I by Zn^{2+} is caused by binding to two high-affinity sites characterized by K_i values of 86 and 50 μM, respectively.

These sites are not freely accessible as indicated by the complex binding. Zn^{2+} binding strongly competes with that of protons, which is in agreement with the data from FT-IR spectroscopy indicating that Zn^{2+} binds to carboxylic acid residues in a hydrophobic environment. In analogy to cytochrome *c* oxidase,[16−18] we propose that Zn^{2+} binds to charged amino acids of the proton translocation pathways. Each pathway consists of two half-channels with one half-channel being open and the other being closed in the oxidized complex and vice versa in its reduced state.[10] Accordingly, the two high-affinity binding sites of Zn^{2+} may correspond to the open half-channels in the oxidized complex and the reduced complex, respectively. Mutagenesis of the conserved charged amino acids in the membrane arm led to either a decreased stability of complex I or a decreased level of proton translocation (see, for example, refs 32−34).

dx.doi.org/10.1021/bi5009276 | *Biochemistry* 2014, 53, 6332−6339

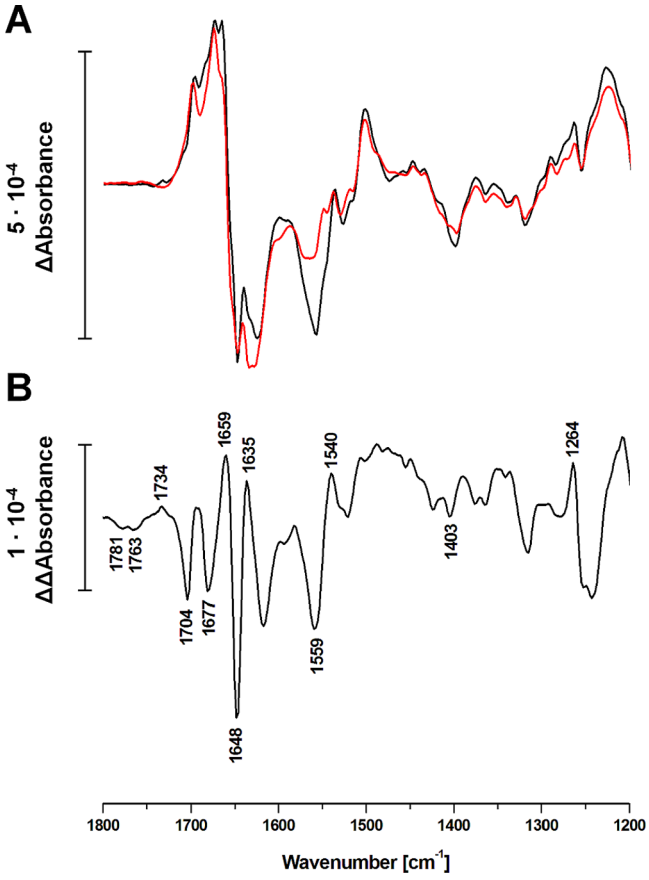

Figure 8. (A) Fully oxidized minus fully reduced difference spectra of untreated (black) and Zn^{2+}-incubated (red) complex I for the step from −500 to 200 mV and (B) double-difference spectrum of the untreated minus the Zn^{2+}-treated sample. The equilibration times for reduction and oxidation were 8 min each.

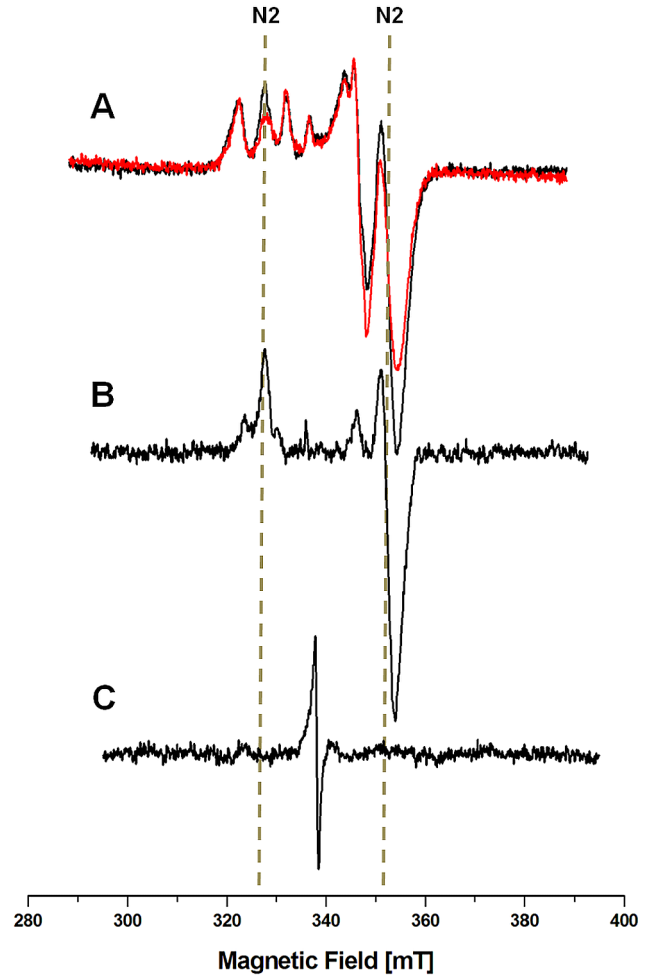

Figure 9. EPR spectra of untreated (A, black) and Zn^{2+}-incubated (A, red) aliquots of complex I at 13 K and 5 mW reduced by NADH. (B) Difference spectrum of the untreated minus the Zn^{2+}-incubated sample. (C) Difference spectrum of the samples reduced by dithionite. The radical signal in spectrum C derives from a slight excess of dithionite in the untreated sample. The positions of the $g_{x,y}$ and g_z signals of cluster N2 are indicated by dotted lines. Other EPR conditions were as follows: microwave frequency, 9.44 GHz; modulation amplitude, 0.6 mT; time constant, 0.164 s; scan rate, 17.9 mT/min.

The energy released by the redox reaction in the peripheral arm has to be transmitted to the membrane arm by conformational changes. The FT-IR difference spectra show that the overall structural flexibility of the complex is significantly decreased in the presence of Zn^{2+}. The differential amide I signal is typical for Fe/S proteins,[30] suggesting that it reflects a decreased structural flexibility around Fe/S cluster N2. This proposal is in agreement with the only partial reduction of N2 by NADH in the presence of Zn^{2+}. This supports the idea of a tight but elastic coupling of electron transfer involving N2 and the quinone with proton translocation.

Our data fit the proposal that Zn^{2+} might exert a common inhibitory mechanism on proton-translocating enzymes by blocking an entry or an exit of a proton translocation pathway. For example, two Zn^{2+}-binding sites were found in chicken complex III.[36] Zinc is causing an inhibition of the complex by binding close to the Q_o center of the complex. One binding site is located in a hydrophobic channel between the Q_o center and the lipid phase, and the other is located between cytochromes *b* and c_1, possibly interfering with the proton pathway to the aqueous phase. The binding clusters were identified by X-ray absorption fine-structure measurements.[37] The ligands of one tetrahedral cluster were identified as two histidine residues, one lysine and an aspartate residue. Homologous bacterial complex III contains an octahedral center consisting of one histidine, one glutamic acid, one aspartic acid, one asparagine, and two water molecules. Zn^{2+} bound to this position seems to block the entrance of a proton release pathway, impairing the function of the histidine residue to act as a proton donor and acceptor. The same mechanism of inhibition was proposed for the bacterial photosynthetic reaction center.[38] Using a combination of enzyme kinetics, isothermal titration calorimetry, and FT-IR difference spectroscopy, we concluded that Zn^{2+} directly binds a conserved glutamic acid residue that is involved in proton efflux coupled to electron transfer at the Q_o center of complex III.[39] Crystallographic studies with bacterial complex IV revealed that the metal-binding site is a glutamic acid residue at the entrance of a proton pathway called the K pathway.[18] Mutants lacking this residue and a nearby histidine residue are devoid of the high-affinity metal-binding site but are still inhibited by Zn^{2+}. Removal of subunit III of this enzyme complex that is known to alter an additional proton pathway called the D pathway eliminates the sensitivity to Zn^{2+}. Thus, a pair of residues, a glutamic acid and a histidine, in subunit II of bacterial complex IV makes up the metal-binding site that is

dx.doi.org/10.1021/bi5009276 | *Biochemistry* 2014, 53, 6332−6339

inhibiting the uptake of protons into the K pathway.[18] We propose a similar binding of Zn^{2+} to *E. coli* respiratory complex I.

AUTHOR INFORMATION

Corresponding Author

*E-mail: friedrich@bio.chemie.uni-freiburg.de. Phone: +49 (0) 761 203 6060. Fax: +49 (0)761 203 6096.

Present Addresses

[§]D.M.: Novartis Vaccines and Diagnostics, Emil-von Behring Str. 76, 35041 Marburg, Germany.

[∥]S.K.: Laboratoire d'Electrochimie Moléculaire, Université Paris Diderot, UMR CNRS 7591, 15, rue Jean-Antoine de Baïf, 75205 Paris Cedex 13, France.

Funding

We thank the Deutsche Forschungsgemeinschaft (DFG), the region Alsace, the institute universitaire de France (IUF), and the FRC-Labex Strasbourg for funding this project.

Notes

The authors declare no competing financial interest.

ABBREVIATIONS

decyl-ubiquinone, 2,3-dimethoxy-5-methyl-6-decyl-benzoquinone; EPR, electron paramagnetic resonance; FMN, flavin mononucleotide; Fe/S, iron−sulfur; FT-IR, Fourier transform infrared; HAR, hexaammineruthenium; IC_{50}, inhibitor concentration needed for half-maximal inhibition of enzyme activity; MES, 2-(*N*-morpholino)ethanesulfonic acid; N2, iron−sulfur cluster N2; SHE, standard hydrogen electrode; $\nu(COO^-)^s$ and $\nu(COO^-)^{as}$, symmetric and asymmetric stretching vibrations, respectively, of the COO^- group of an acidic residue; $\nu(C{=}O)$, stretching vibration of a carbonyl group.

REFERENCES

(1) Ohnishi, T. (1998) Iron-sulfur clusters/semiquinones in complex I. *Biochim. Biophys. Acta 1364*, 186−206.

(2) Friedrich, T. (2001) Complex I: A chimaera of a redox and conformation-driven proton pump? *J. Bioenerg. Biomembr. 33*, 169−177.

(3) Brandt, U. (2006) Energy converting NADH:quinone oxidoreductase (complex I). *Annu. Rev. Biochem. 75*, 69−92.

(4) Sazanov, L. A. (2007) Respiratory complex I: Mechanistic and structural insights provided by the crystal structure of the hydrophilic domain. *Biochemistry 46*, 2275−2288.

(5) Hirst, J. (2013) Mitochondrial complex I. *Annu. Rev. Biochem. 82*, 551−575.

(6) Dawson, T. M., and Dawson, V. L. (2003) Molecular pathways of neurodegeneration in Parkinson's disease. *Science 302*, 819−822.

(7) Balaban, R. S., Nemoto, S., and Finkel, T. (2005) Mitochondria, oxidants, and aging. *Cell 120*, 483−495.

(8) Friedrich, T. (1998) The NADH:ubiquinone oxidoreductase (complex I) from *Escherichia coli*. *Biochim. Biophys. Acta 1364*, 134−146.

(9) Yagi, T., and Matsuno-Yagi, A. (2003) The proton-translocating NADH-quinone oxidoreductase in the respiratory chain: The secret unlocked. *Biochemistry 42*, 2266−2274.

(10) Baradaran, R., Berrisford, J. M., Minhas, G. S., and Sazanov, L. A. (2013) Crystal structure of the entire respiratory complex I. *Nature 494*, 443−448.

(11) Frederickson, C. J., and Bush, A. I. (2001) Synaptically released zinc: Physiological functions and pathological effects. *BioMetals 14*, 353−366.

(12) Sheline, C. T., Behrens, M. M., and Choi, D. W. (2000) Zinc-induced cortical neuronal death: Contribution of energy failure attributable to loss of NAD^+ and inhibition of glycolysis. *J. Neurosci. 20*, 3139−3146.

(13) Gazaryan, I. G., Krasnikov, B. F., Ashby, G. A., Thorneley, R. N. F., Kristal, B. S., and Brown, A. M. (2002) Zinc is a potent inhibitor of thiol oxidoreductase activity and stimulates reactive oxygen species production by lipoamide dehydrogenase. *J. Biol. Chem. 277*, 10064−10072.

(14) Sharpley, M. S., and Hirst, J. (2006) The Inhibition of Mitochondrial Complex I (NADH:Ubiquinone Oxidoreductase) by Zn^{2+}. *J. Biol. Chem. 281*, 34803−34809.

(15) Link, T. A., and von Jagow, G. (1995) Zinc ions inhibit the Q_P center of bovine heart mitochondrial bc_1 complex by blocking a protonatable group. *J. Biol. Chem. 270*, 25001−25006.

(16) Aagaard, A., and Brzezinski, P. (2001) Zinc ions inhibit oxidation of cytochrome *c* oxidase by oxygen. *FEBS Lett. 494*, 157−160.

(17) Kannt, A., Ostermann, T., Müller, H., and Ruitenberg, M. (2001) Zn^{2+} binding to the cytoplasmic side of *Paracoccus denitrificans* cytochrome *c* oxidase selectively uncouples electron transfer and proton translocation. *FEBS Lett. 503*, 142−146.

(18) Qin, L., Mills, D. A., Hiser, C., Murphree, A., Garavito, R. M., Ferguson-Miller, S., and Hosler, J. (2007) Crystallographic location and mutational analysis of Zn and Cd inhibitory sites and role of lipidic carboxylates in rescuing proton path mutants in cytochrome *c* oxidase. *Biochemistry 46*, 6239−6248.

(19) Pohl, T., Uhlmann, M., Kaufenstein, M., and Friedrich, T. (2007) Lambda Red-mediated mutagenesis and efficient large scale affinity purification of the *Escherichia coli* NADH:ubiquinone oxidoreductase (complex I). *Biochemistry 46*, 10694−10702.

(20) Hellwig, P., Scheide, D., Bungert, S., Mäntele, W., and Friedrich, T. (2000) FT-IR spectroscopic characterization of NADH:ubiquinone oxidoreductase (complex I) from *Escherichia coli*: Oxidation of Fe/S cluster N2 is coupled with the protonation of an aspartate or glutamate side chain. *Biochemistry 39*, 10884−10891.

(21) Birrell, J. A., King, M. S., and Hirst, J. (2011) A ternary mechanism for NADH oxidation by positively charged electron acceptors, catalyzed at the flavin site in respiratory complex I. *FEBS Lett. 585*, 2318−2322.

(22) Wolpert, M., and Hellwig, P. (2006) Infrared spectra and molar absorption coefficients of the 20 α amino acids in aqueous solutions in the spectral range from 1800 to 500 cm^{-1}. *Spectrochim. Acta, Part A 64A*, 987−1001.

(23) Barth, A. (2001) The infrared absorption of amino acid side chains. *Prog. Biophys. Mol. Biol. 74*, 141−173.

(24) Zhang, J., Oettmeier, W., Gennis, R. B., and Hellwig, P. (2002) FTIR spectroscopic evidence for the involvement of an acidic residue in quinone binding in cytochrome *bd* from *Escherichia coli*. *Biochemistry 41*, 4612−4617.

(25) Hellwig, P., Gomes, C. M., and Teixeira, M. (2003) FTIR spectroscopic characterization of the cytochrome aa_3 from *Acidianus ambivalens*: Evidence for the involvement of acidic residues in redox coupled proton translocation. *Biochemistry 42*, 6179−6184.

(26) Nara, M., Torii, H., and Tasumi, M. (1996) Correlation between the vibrational frequencies of the carboxylate group and the types of its coordination to a metal ion: An *ab initio* molecular orbital study. *J. Phys. Chem. 100*, 19812−19817.

(27) Neehaul, Y., Juárez, O., Barquera, B., and Hellwig, P. (2013) Infrared Spectroscopic Evidence of a Redox-Dependent Conformational Change Involving Ion Binding Residue NqrB-D397 in the Na^+-Pumping NADH:Quinone Oxidoreductase from *Vibrio cholerae*. *Biochemistry 52*, 3085−3093.

(28) Arrondo, J. L. R., Muga, A., Castresana, J., and Goni, F. M. (1993) Quantitative studies of the structure of proteins in solution by Fourier-transform infrared spectroscopy. *Prog. Biophys. Mol. Biol. 59*, 23−56.

(29) Goormaghtigh, E., Cabiaux, V., and Ruysschaert, J. M. (1994) Determination of soluble and membrane protein structure by Fourier transform infrared spectroscopy. III. Secondary structures. *Subcell. Biochem. 23*, 405−450.

(30) Friedrich, T., and Hellwig, P. (2010) Redox-induced conformational changes within the *Escherichia coli* NADH ubiquinone oxidoreductase (complex I): An analysis by mutagenesis and FT-IR spectroscopy. *Biochim. Biophys. Acta 1797*, 659−663.
(31) Berrisford, J. M., and Sazanov, L. A. (2009) Structural basis for the mechanism of respiratory complex I. *J. Biol. Chem. 284*, 29773−29783.
(32) Sinha, P. K., Torres-Bacete, J., Nakamaru-Ogiso, E., Castro-Guerrero, N., Matsuno-Yagi, A., and Yagi, T. (2009) Critical roles of subunit NuoH (ND1) in the assembly of peripheral subunits with the membrane domain of *Escherichia coli* NDH-1. *J. Biol. Chem. 284*, 9814−9823.
(33) Kervinen, M., Hinttala, R., Helander, H. M., Kurki, S., Uusimaa, J., Finel, M., Majamaa, K., and Hassinen, I. E. (2006) The MELAS mutations 3946 and 3949 perturb the critical structure in a conserved loop of the ND1 subunit of mitochondrial complex I. *Hum. Mol. Genet. 15*, 2543−2552.
(34) Michel, J., DeLeon-Rangel, J., Zhu, S., Van Ree, K., and Vik, S. B. (2011) Mutagenesis of the L, M, and N subunits of Complex I from *Escherichia coli* indicates a common role in function. *PLoS One*, e17420.
(35) Morina, K., Schulte, M., Hubrich, F., Dörner, K., Steimle, S., Stolpe, S., and Friedrich, T. (2011) Engineering the respiratory complex I to an energy-converting NADPH:ubiquinone oxidoreductase. *J. Biol. Chem. 286*, 34267−34634.
(36) Berry, E. A., Zhang, Z., Bellamy, H. D., and Huang, L. (2000) Crystallographic location of two Zn^{2+}-binding sites in the avian cytochrome bc_1 complex. *Biochim. Biophys. Acta 1459*, 440−448.
(37) Giachini, L., Francia, F., Veronesi, G., Lee, D. W., Daldal, F., Huang, L. S., Berry, E. A., Cocco, T., Papa, S., Boscherini, F., and Venturoli, G. (2007) X-ray absorption studies of Zn^{2+} binding sites in bacterial, avian, and bovine cytochrome bc_1 complexes. *Biophys. J. 93*, 2934−2951.
(38) Axelrod, H. L., Abresch, E. C., Paddock, M. L., Okamura, M. Y., and Feher, G. (2000) Determination of the binding site of the proton transfer inhibitors Cd^{2+} and Zn^{2+} in bacterial reaction centers. *Proc. Natl. Acad. Sci. U.S.A. 97*, 1542−1547.
(39) Lee, D. W., El Khoury, Y., Francia, F., Zambelli, B., Ciurli, S., Venturoli, G., Hellwig, P., and Daldal, F. (2011) Zinc inhibition of bacterial cytochrome bc_1 reveals the role of cytochrome *b* E295 in proton release at the Q_o site. *Biochemistry 50*, 4263−4272.